# On Spreading Resistance for an Isothermal Source on a Compound Flux Channel

### Hiroyuki Miyoshi

Toby L. Kirk

Graduate School of School of Mathematical Sciences Information Science and Technology, The University of Tokyo 113-8656, Hongo, 7-3-1, Bunkyo-ku Tokyo, Japan

Email: hiroyukimiyoshi@g.ecc.u-tokyo.ac.jp

SO17 1BJ, University Rd Southampton, UK

University of Southampton

### **Marc Hodes**

Department of Mechanical Engineering Department of Mathematics **Tufts University** Medford MA 02155, USA

#### **ABSTRACT**

Recently, Jain [ASME J. Heat Mass Transfer, 220 (2024)] provided spreading-resistance formulas for an isothermal source on compound, orthotropic, semi-infinite, two-dimensional (axisymmetric) flux channels (tubes). The boundary condition (BC) in the source plane was a discontinuous convection (Robin) one. Along the source, a sufficiently-large heat transfer coefficient was imposed to approximate an isothermal condition; elsewhere, it was set to zero, imposing an adiabatic BC. An eigenfunction expansion resolved the problem. Distinctly, we impose, precisely, a mixed isothermal-adiabatic BC in the source plane and use conformal maps to resolve the spreading resistance for the limiting case of a compound, isotropic flux channel. Our complimentary approach requires more time to compute the spreading resistance. However, it converges uniformly rather than pointwise, converges to the exact spreading resistance rather than one with an error, eliminates the Gibbs phenomenon at the edges of the source and fully resolves the square-root singularities in heat flux as the discontinuity in the BC is approached.

### **NOMENCLATURE**

- $T^*$  (dimensional) temperature (K)
- $T_s^*$  (dimensional) source temperature (K)
- $x^*$  (dimensional) coordinate (m)
- $y^*$  (dimensional) coordinate (m)
- $2b^*$  total width of channel (m)
- $2a^*$  total width of source region (m)
- $h^*$  height of the first layer (m)
- $k_1$  thermal conductivity of the first layer (W/m·K)
- $k_2$  thermal conductivity of the second layer (W/m·K)
- z + iy
- $h_1(z)$  analytic extension of  $\theta_1$
- $h_2(z)$  analytic extension of  $\theta_2$
- $D_{\zeta}$  triply connected domain in Figure 3
- $\theta_1$  non-dimensional temperature of the first layer
- $\theta_2$  non-dimensional temperature of the second layer
- $\sigma k_1/k_2$
- $a \quad a^*/b^*$
- $h \quad h^*/b^*$
- $x \quad x^*/b^*$
- $y \quad y^*/b^*$

### 1 INTRODUCTION

Spreading (constriction) resistance results when heat is conducted from (to) a finite region to (from) a larger one because of the finite, "in-plane" thermal conductivity of all materials. It

is important in a myriad of applications in heat transfer [1]. These include electronics packaging [2], conduction in the base of a heat sink [3] and thermal contact resistance [4]. Moreover, its mathematical-equivalent is common in many physical problems, as discussed by Hodes et al. [5]. For example, as discussed further below, it is encountered in the problems of finding the apparent hydrodynamic and thermal slip lengths characterizing a superhydrophobic surface [6].

A new monograph by Muzychka and Yovanovich [1] discusses the extensive body of virtually all known analytical and semi-analytical solutions for spreading resistance and their applications. Such solutions, including that considered here, are extremely valuable relative to numerical ones. For example, in the design of GaN-on-diamond high electron-mobility transistors, Bagnall and Muzychka [7] showed that their semi-analytical formula required an order-of-magnitude smaller computation time than finite-element solutions. Given the new monograph [1], we only discuss those studies relevant to the present work on the two-dimensional conduction problem of an isothermal strip in an otherwise adiabatic source plane on a semi-infinite flux channel.

Before considering compound, semi-infinite, two-dimensional flux channels, we discuss solutions for a single-material one. Figure 1 (a) illustrates this conduction problem, governed by Laplace's equation, for an isothermal source at a temperature  $T_{\rm s}^*$  and of width  $2a^*$  centered in the middle  $(x^*=0)$  of the base  $(y^*=0)$  of a  $2b^*$ -wide flux channel. The remaining boundaries of the domain are adiabatic, except for a constant far-field heat flux,  $q^*$ . The thermal conductivity of the material is k. In the dimensionless analogue of the problem shown in Figure 1 (b), we drop the asterisks on relevant quantities, all lengths are non-dimensionalized by  $b^*$  and  $T=T^*k/(q^*b^*)$ .

The mathematical equivalent of this problem, i.e., a constant, homogeneous Dirichlet boundary condition (BC) on an otherwise constant, homogeneous Neumann BC finite-width plane in a semi-infinite medium with a constant far-field Neumann BC satisfying Laplace's equation, is common in physics. Indeed, in 1939, Smythe [8], in the context of electrostatics, resolved the voltage field. He did not, however, use his results to provide an expression for spreading resistance.

Turning to experiments, at least as early as 1949, spreading resistance in a closely-related problem was measured. To be sure, in the context of electrostatics, i.e., the effect of electrical contact resistance on resistance welding, Kouwenhoven and Sackett [9] measured it in electrical

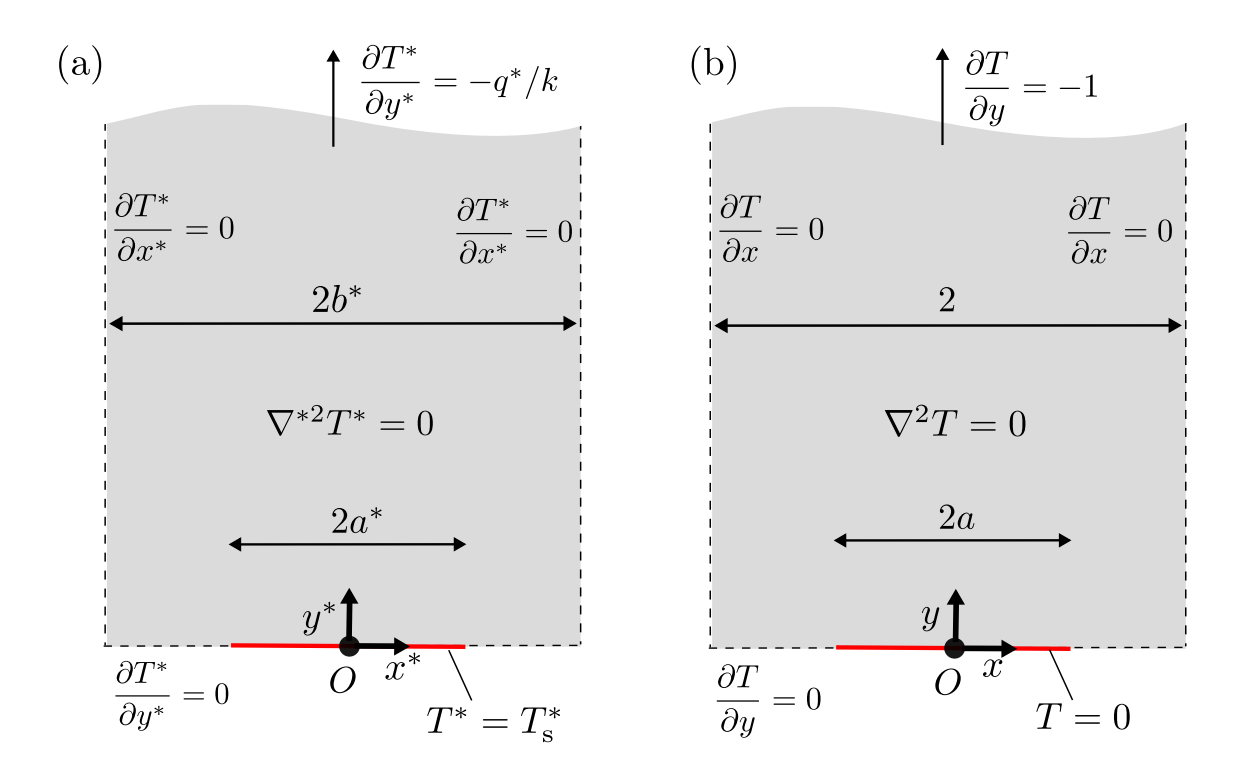


Fig. 1. (a) Dimensional and (b) dimensionless problems for a single-material, isotropic, semi-infinite flux channel.

experiments in the "abrupt change" configuration. Correspondingly, their specimens were metal bars of rectangular-cross section with a finite-length constriction, also rectangular in cross section, between the ends. The spreading resistance of such an abrupt change in a rectangular cross-sectional area flux channel, where both the constricted and non-constricted regions are semi-infinite has been resolved by Smythe [8]. In the limit that the ratio of the widths of the constricted-to-non-constricted portions of the strip approaches zero, the spreading resistance is given by a later-developed formula (1) discussed below. (Relatedly, the almost isothermal BC utilized by Mikic [10], also discussed below, becomes valid.) Conversely, as this ratio becomes sufficiently large, the increase in spreading resistance relative to the case of an isothermal strip in a semi-infinite domain is dramatic [1]. However, both spreading resistances, of course, vanish as the ratio approaches 1. Notably, in some experiments by Kouwenhoven and Sackett [9], the constriction was eccentric, i.e., not centered along the base of the domain. Finally, in a subsequent study, Kouwenhoven and Sackett [11] verified their experiments were consistent with the solution by Smythe [8].

The analytical solution to the problem depicted in Fig. 1, as mentioned by Muratov and Stanislov [12], also traces back to a publication in 1955 by Moizhes [13], again in the context of electrostatics. He was the first to provide the formula for spreading resistance,  $R_{\rm sp}^*$ , i.e., for our purposes, the additional temperature rise of the source relative to the one-dimensional problem, where it spans the whole width of the domain, per unit heat rate in  ${}^{\circ}$ C/W. The formula is

$$kL^*R_{\rm sp}^* = \frac{1}{\pi}\log\left[\csc\left(\frac{\pi a}{2}\right)\right],\tag{1}$$

where  $L^*$  is the depth of the flux channel.

Analysis in a heat conduction context traces back to Mikic [10]. He resolved, via separation of variables, the problem of an isoflux source in an otherwise adiabatic source plane, i.e., he imposed a discontinuous rather than mixed BC. Clearly, there is no singularity in heat flux normal to the source plane. Hodes *et al.* [14] expressed Mikic's results for spreading resistance, based on the mean or maximum source temperature, in terms of polylogarithm functions. Moreover, Li and Lu [15] provide, in polar  $(r, \theta)$  coordinates, the temperature field, local to the discontinuity. Imposing an adiabatic condition at  $\theta = 0$  and finite and constant heat flux source at  $\theta = \pi$ , it manifests itself, dimensionlessly, as

$$T = \frac{r}{\pi} \left[ \log(r) \cos(\theta) - \theta \sin(\theta) \right] + \sum_{k=0}^{\infty} a_k r^k \cos(k\theta).$$

Here,  $T=T^*k/(q^*a^*)$ ,  $r=r^*/a^*\ll 1$  and the constant coefficients  $a_k$  require the full solution. In Cartesian local coordinates  $(x=x^*/a^*,y=y^*/a^*)$  relative to the singularity at x=0 in the source plane (y=0),

$$T = \frac{x \ln|x|}{\pi} + \sum_{k=0}^{\infty} a_k |x|^k \cos \theta.$$
 (2)

Consequently, the heat flux in the source plane exhibits an  $\mathcal{O}(r \log r)$  singularity from any direction, except  $\pi/2$ , as x approaches the discontinuity in the BC along the source plane.

Mikic next resolved, again, by separation of variables, the spreading resistance corresponding to what is, today, sometimes referred to as an "almost isothermal" BC, i.e., the heat flux along the source is proportional to  $1/\sqrt{a^2-x^2}$ . Moreover, albeit not mentioned in the relevant literature, he also resolved the temperature field for the case of an isothermal source using a conformal map. He, like Smythe [8], did not manipulate it to find spreading resistance but did use it to provide two important results. First, he provided an exact formula for the heat flux over the isothermal portion of the source plane. Secondly, he showed that (after manipulation of his Equation (D.16)) the temperature profile over an almost isothermal source is accurate to  $\mathcal{O}(a)$ .

Proceeding chronologically, in 1968, Veziroglu and Chandra [16], unaware of the study by Moizhes [13], independently resolved the formula (1) for spreading resistance. They also considered an eccentric heat source but for a constant heat flux rather than isothermal BC. Shortly thereafter Veziroglu and Huerta [17] resolved the problem for an eccentric, isothermal source, as did Sexl and Burkhard [18] soon thereafter.

This brings us to the seminal work by Philip [19, 20] in the context of the hydrodynamic BC at fluid-fluid interfaces in porous media. He provided the perturbation to the velocity field for "clean" (mobile/shear-free) interfaces relative to "dirty" (immobile/no slip) ones in a myriad of flow configurations. Clearly, by dirty interfaces he was referring to those where the buildup of surfactants along them immobilized them — see, e.g., Palaparthi *et al.* [21] for a discussion of the relevant physics. One of the problems he considered was a linear-shear flow over a plate with a periodic array of no-shear slots, the mathematical equivalent of the problem first resolved by Smythe [8] insofar as the field and Moizhes [13] insofar as the perturbation to it at infinity, which led to, yet again, (1). We note that the temperature field given by Mikic [10] and the velocity field given by Philip [19], although distinct in form, are, of course, identical as shown in the Appendix A. We further note that Philip's problem is best viewed in terms of a constriction rather than spreading resistance context as the no-slip BC is a momentum sink.

It is noteworthy that, in recent years, the foregoing work has had an enormous impact on

the analysis of the flow and heat transfer in adiabatic and diabatic microchannels textured with superhydrophobic surfaces. Representatively, Hodes *et al.* [14] used the results of the mixed BC problem for the inner hydrodynamic problem and the discontinuous Neumann BC (first result by Mikic [10]) for the inner thermal problem to resolve the flow and heat transfer in a diabatic, superhydrhophobic microchannel via matched asymptotics. Moreover, as first studied in depth by Peaudecerf *et al.* [22], immobilization of portions or all of menisci by surfactants, precisely the physical mechanism of interest to Philip [19, 20], formed in superhydrophobic microchannels is responsible for the reduced drag relative to the shear-free limit in most experimental studies [23].

More recent studies have progressed beyond the foregoing canonical problems. As discussed by Hodes *et al.* [5], combining the results of Schnitzer [24] and Crowdy [25] provides formula for the spreading resistance when the adiabatic portion of the bottom of the domain is a circular arc, thereby capturing the effects of surface roughness. Moreover, again in the context of a flow over superhydrophobic surface, Crowdy [26] resolved the spreading resistance for an arbitrary array of isothermal and adiabatic BCs in the source plane in a period window and, subsequently, extended his result to the case of weakly-curved, circular arcs in [5]. Notably, Mayer *et al.* [27] used the first result by Crowdy [26] in their resolution of thermocapillary-driven flow through a superhydrophobic microchannel. Moreover, the present result would constitute the inner hydrodynamic problem in the context a flow of a layer of two liquids through a superhydrophobic microchannel (see Hodes *et al.* [5] for the single fluid case). Finally, when the source is constant heat flux rather than isothermal, Lam *et al.* [28], using a boundary perturbation, resolved the problem when the adiabatic portion of the bottom of the domain is a weakly-curved circular arc.

The only result for spreading and constriction resistance for an isothermal source on a compound flux channel is that by Jain [29]. Notably, a suite of related problems is resolved when the source is isoflux [1], which simplifies the mathematics. For example the three-dimensional problem for a rectangular source on a compound, orthotropic, finite-thickness flux channel with an interfacial resistance between the layers and a convection BC in the sink plane has been resolved by Muzychka [30]. Returning to the problem at hand, Jain [29] resolved the two-dimensional and semi-infinite Cartesian (isothermal strip in source plane) and axisymmetric (isothermal circle in

source plane) cases. The thermal conductivities in both regions of the channel were orthotropic; therefore, materials such as pyrolytic graphite that are used in the thermal management of electronics may be accommodated. Representatively, HPMS Graphite (Woodland, CA), sells flexible, low-density graphite sheet in their HGS series with "in-plane" thermal conductivities up to 1800 W/(mK) and "through-plane" ones between 10 and 26 W/(mK). Jain [29] resolved the mixed BCs in the source plane by utilizing a discontinuous convection BC. The heat transfer coefficient was very large over the source to approximate it as isothermal. It was zero elsewhere in the source plane to render it adiabatic.

There are many physical configurations where the spreading resistance in compound flux channels is relevant. For example, soft metallic coatings are used to reduce thermal contact resistance between mating surfaces [31]. Representatively, Kang et al. [32] increased, by up to a factor of 7, the thermal contact conductance of joints between Aluminum 6061 T6 surfaces by coating them with micron-scale thickness, vapor-deposited lead, tin or indium. N.b., there is an optimal thickness of such coatings because, although they are relatively soft such that contact area increases, they are less conductive than Aluminum. Moreover, the bases of Aluminum heat sinks are often anodized to increase their emissivity and corrosion resistance, provide dielectric isolation and enable, for aesthetics, absorption of colored dyes. The porous metal-oxide layer formed by anodization is often tens of microns thick. In such applications, the lower "thin film" region of the compound flux channel can not be considered semi-infinite. Indeed, conduction is multi-dimensional until a perpendicular distance from the source plane of about the width of the flux channel. Therefore, the coupled problem, where varying temperature and heat flux are matched at the interface, needs to be resolved.

We consider an isotropic compound flux channel but impose a true isothermal-adiabatic (Dirichlet-Neumann) mixed BC in the source plane to complement the study by [29]. Via complex analysis, we fully resolve the aforementioned square-root singularity in heat flux as the change from a Dirichlet to Neumann BC in the source plane is approached. Specifically, requisite conformal maps are developed using Schottky-Klein prime functions, subsequently referred to as prime functions, tailored to multiply connected domains. Using them and a technique for solving mixed boundary

value problems for multiply connected domains described by Miyoshi *et al.* [33, 34], we derive a linear system for the coefficients of the temperature field. They are easily evaluated by code available on github [35] and a sample code for computing them is provided in Appendix C.

The rest of this paper is organized as follows: Section 2 presents the mathematical formulation of the mixed boundary-value problem. Section 3 calculates spreading resistances and numerical results are presented in Section 4 followed by a Discussion in Section 5.

### **2 PROBLEM FORMULATION**

Following Jain [29], we formulate the problem for heat conduction from an isothermal source on a compound, semi-infinite, two-dimensional flux channel as per Fig. 2. However, our materials are isotropic rather than orthotropic. The source is  $2a^*$  wide and its temperature is denoted by  $T_s^*$ . The source plane  $(y^* = 0)$  is otherwise adiabatic and of total width  $2b^*$ . The origin is the center of the source. The lower material (domain  $D_1$ ) is of finite thickness  $h^*$  and of thermal conductivity  $k_1$ . The upper one (domain  $D_2$ ) is semi-infinite and of thermal conductivity  $k_2$ . The temperature fields  $T_1^*(x^*,y^*)$  and  $T_2^*(x^*,y^*)$  satisfy Laplace's equation as per

$$k_1 \left( \frac{\partial^2 T_1^*}{\partial x^{*2}} + \frac{\partial^2 T_1^*}{\partial y^{*2}} \right) = 0, \tag{3}$$

$$k_2 \left( \frac{\partial^2 T_2^*}{\partial x^{*2}} + \frac{\partial^2 T_2^*}{\partial y^{*2}} \right) = 0.$$
 (4)

Turning to the BCs, the isothermal source is defined by

$$T_1^*(x^*, 0) = T_s^*, \quad -a^* < x^* < a^*.$$
 (5)

The adiabatic boundaries outside the source region in the source plane and on the sides of the

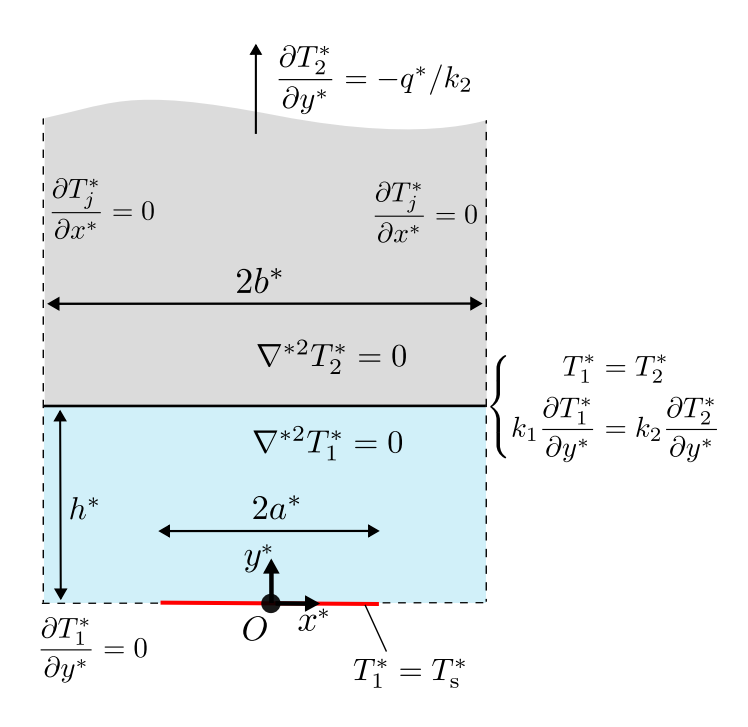


Fig. 2. Isothermal source on a compound, isotropic, semi-infinite, two-dimensional flux channel.

domain manifest themselves as

$$\frac{\partial T_1^*}{\partial y^*}(x^*, 0) = 0, \quad -b^* \le x^* \le -a^*, \quad a^* \le x^* \le b^*$$
 (6)

$$\frac{\partial T_1^*}{\partial x^*}(\pm b^*, y^*) = 0, \quad 0 \le y^* \le h^*, \tag{7}$$

$$\frac{\partial T_2^*}{\partial x^*}(\pm b^*, y^*) = 0, \quad y^* > h^*. \tag{8}$$

On the interface between the materials, temperature and heat flux continuity read

$$\begin{cases}
T_1^*(x^*, h^*) = T_2^*(x^*, h^*), \\
k_1 \frac{\partial T_1^*}{\partial y^*}(x^*, h^*) = k_2 \frac{\partial T_2^*}{\partial y^*}(x^*, h^*),
\end{cases}$$
(9)

for  $-b^* \le x^* \le b^*$ . A constant heat flux BC holds in the far-field as per

$$\frac{\partial T_2^*}{\partial y^*} \to -q^*/k_2, \quad y^* \to \infty. \tag{10}$$

We define the following non-dimensional variables

$$\begin{cases} \theta_{j} = (T_{j}^{*} - T_{s}^{*}) \cdot \frac{k_{2}}{q^{*}b^{*}}, \ j = 1, 2, \\ \sigma = k_{1}/k_{2}, \\ (x, y) = (x^{*}/b^{*}, y^{*}/b^{*}), \\ (a, h) = (a^{*}/b^{*}, h^{*}/b^{*}). \end{cases}$$

$$(11)$$

The dimensionless form of the problem becomes, as depicted in Fig. 3,

$$abla^2 \theta_1 = 0, \quad (x, y) \in D_1,$$
 (12)

$$\nabla^2 \theta_2 = 0, \quad (x, y) \in D_2, \tag{13}$$

with

$$\begin{cases} \theta_{1}(x,0) = 0, & -a \leq x \leq a, \\ \frac{\partial \theta_{1}}{\partial y}(x,0) = 0, & a \leq |x| \leq 1, \\ \frac{\partial \theta_{1}}{\partial x}(\pm 1, y) = 0, & 0 \leq y \leq h, \\ \frac{\partial \theta_{2}}{\partial x}(\pm 1, y) = 0, & y \leq \infty, \end{cases}$$

$$(14)$$

where  $D_1 \equiv \{(x,y) | -1 \le x \le 1, 0 \le y \le h\}$ , and  $D_2 \equiv \{(x,y) | -1 \le x \le 1, h \le y \le \infty\}$  and the

On Spreading Resistance for an Isothermal Source on a Compound Flux Channel

continuity conditions (9) are

$$\begin{cases} \theta_1 = \theta_2, \\ \sigma \frac{\partial \theta_1}{\partial y} = \frac{\partial \theta_2}{\partial y}. \end{cases} \tag{15}$$

The far-field condition (10) becomes

$$\theta_2 \to -y + \text{constant} + \mathcal{O}(1/z), \quad \text{as } y \to \infty,$$
 (16)

where  $z \equiv x + iy$ . It ensures the uniqueness of the solution [29].

Jain [29] used Fourier expansions of  $\theta_1$  and  $\theta_2$ , obtaining linear systems for Fourier coefficients. Rather than resolving the mixed boundary condition on y=0, he considered a discontinuous convection boundary condition, where the Biot number (dimensionless heat transfer coefficient) was very large in the isothermal region and zero in the adiabatic one. However, because of the square-root singularity on this boundary at  $x=\pm a$ , a large number of coefficients was necessary and the singularity is not fully resolved.

#### 3 SPREADING RESISTANCE

This section summarizes our result for spreading resistances obtained from complex analysis. In dimensional form, the spreading resistance is [1]

$$R_{\rm sp} = \frac{T_{\rm s}^* - T_{\rm average}^*}{Q^*} \tag{17}$$

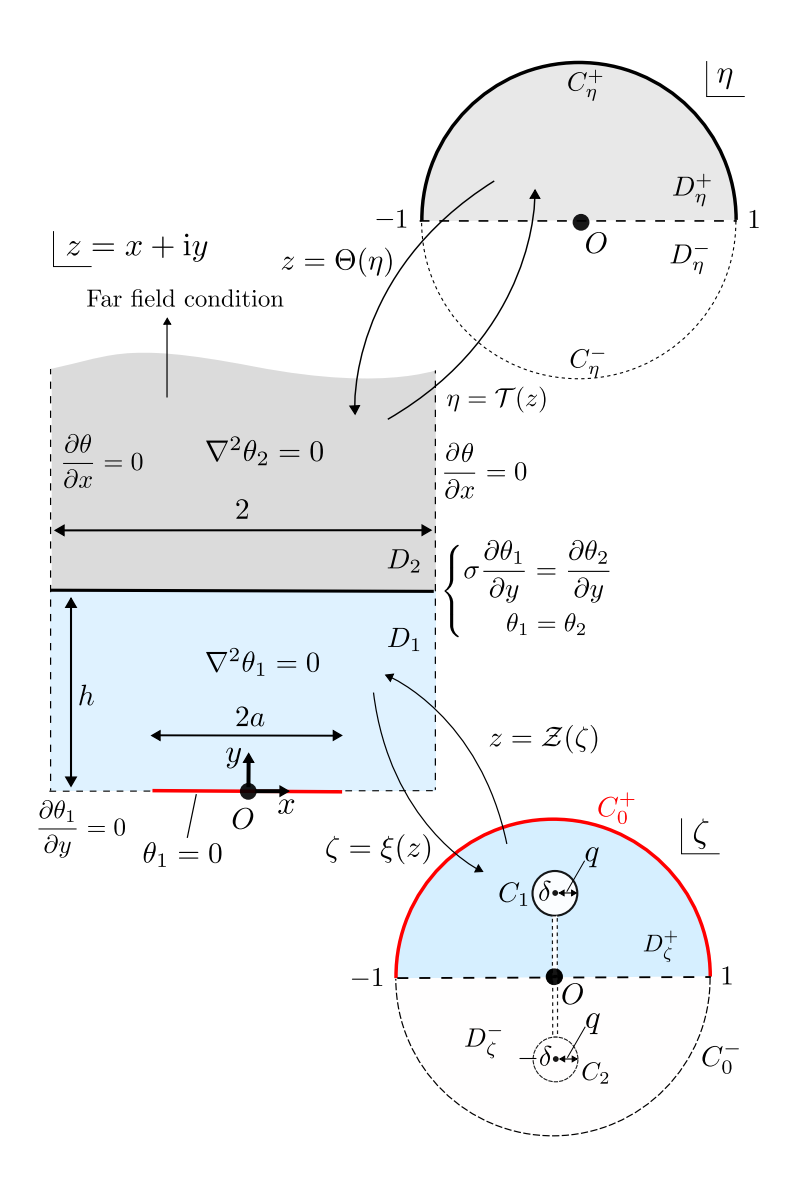


Fig. 3. Non-dimensional geometry and two conformal mappings. The map  $z=\Theta(\eta)$  maps the upper-half disc to the period region  $D_2$ , and the map  $z=\mathcal{Z}(\zeta)$  maps the upper-half disc outside  $C_1$  to the period region  $D_1$ .

where  $T_{\text{average}}^*$  is the average temperature in the plane of the source on  $y^* = 0$  and  $Q^*$  is the heat rate into  $D^*$ , i.e., for a unit-depth domain,

$$Q^* = -2 \int_0^{b^*} k_2 \left(\frac{\partial T^*}{\partial z^*}\right)_{z^* \to \infty} dx^*.$$
(18)

The non-dimensional spreading resistance is given by

$$k_2 b^* R_{\rm sp} = -\frac{1}{2} \theta_{\rm average}(x, 0), \tag{19}$$

where the average  $\theta_{\text{average}}$  on y=0 is given by

$$\theta_{\text{average}} = \int_0^1 \theta_1(x, 0) dx, \tag{20}$$

which is easily calculated after we obtain  $\theta_1$  on the source plane.

We proceed by summarizing our approach for obtaining the spreading resistance as detailed in Appendix B. Since  $\theta_1$  is harmonic, it is convenient to define an analytic extension of  $\theta_1$  as  $h_1(z)=\chi_1+\mathrm{i}\theta_1$  in the complex  $z=x+\mathrm{i}y$ -plane. Because there exist singularities at  $x\pm a$ , we use a special basis of complex function  $\mathcal{Q}_n(\xi(z))$ , which removes these singularities safely using a conformal mapping approach. Consider a truncated Fourier expansion of  $h_1(z)$  as the basis of a complex function  $\mathcal{Q}_n(\xi(z))$  as follows:

$$h_1(z) = \sum_{n=0}^{N-1} a_n \mathcal{Q}_n(\xi(z)),$$
 (21)

where  $Q_n(\zeta)$  satisfies boundary conditions

$$\operatorname{Im}[\mathcal{Q}_{n}(\zeta)] \equiv g_{n}(\zeta) = \begin{cases} 0, & \zeta \in C_{0}, \\ \cos(n\pi \operatorname{Re}[\mathcal{Z}(\zeta)]), & \zeta \in C_{1}, \\ \cos(n\pi \operatorname{Re}[\mathcal{Z}(\overline{\zeta})]), & \zeta \in C_{2}, \end{cases}$$
(22)

and  $\zeta=\xi(z)$  is an inverse of the conformal map  $z=\mathcal{Z}(\zeta)$  in Figure 3. (Note that  $\mathcal{Q}_n(\zeta)$  can

be computed by the Schwarz integral formula (23) with boundary data (22) for triply connected domains.) This boundary value problem can be solved by the Schwarz integral formula [36] using the prime function  $\omega(.,.)$  and the integral of the first kind, i.e.,

$$Q_n(\zeta) = \frac{1}{2\pi} \sum_{j=0}^2 \oint_{C_j} \hat{g}_n(\zeta') d(\log \omega(\zeta, \zeta') + \log \omega(\zeta, 1/\overline{\zeta'}))$$

$$+ \alpha(v_1(\zeta) + v_2(\zeta)) + c_1, \quad \alpha, c_1 \in \mathbb{R},$$
(23)

where  $v_1(\zeta)$  and  $v_2(\zeta)$  are the integrals of the first kind associated to  $C_1$  and  $C_2$ . These special functions  $\omega(.,.),\,v_1(\zeta),\,$  and  $v_2(\zeta)$  can be calculated easily by Github code [35]. The parameter  $\alpha$  is determined by the coupling equations of  $h_1(z)$  and  $h_2(z),\,$  and  $c_1$  is an arbitrary real parameter. The function  $\hat{g}_n(\zeta)$  in (23) satisfies

$$\hat{g}_{n}(\zeta) = \begin{cases} -\alpha \operatorname{Im}[v_{1}(\zeta) + v_{2}(\zeta)], & \zeta \in C_{0}, \\ \cos(n\pi \operatorname{Re}[\mathcal{Z}(\zeta)]) - \alpha \operatorname{Im}[v_{1}(\zeta) + v_{2}(\zeta)], & \zeta \in C_{1}, \\ \cos(n\pi \operatorname{Re}[\mathcal{Z}(\overline{\zeta})]) - \alpha \operatorname{Im}[v_{1}(\zeta) + v_{2}(\zeta)], & \zeta \in C_{2}, \end{cases}$$
(24)

where  $\alpha$  is given by a single-valuedness condition for multiply connected domains [36]. The spreading resistance is then evaluated from  $\theta_1 = \text{Im}[h_1(z)]$  and (20) after calculating the coefficients  $a_n$ ,  $n = 0, \ldots, N-1$  in (21).

We emphasize that the singularities at  $x=\pm a$  are eliminated when we evaluate the Schwarz integral. Indeed, by using a conformal map  $z=\mathcal{Z}(\zeta)$  which maps  $\zeta=\pm 1$  to the edge  $z=\mp a$  and the Schwarz reflection principle, the Schwarz integral has no singularities along the integral path. This technique for the singularity removal is explained in detail in [37].

To obtain the coefficients  $a_n$ , the complex form of continuity conditions (15) are used. We choose N evaluating points  $z_n = x_n + \mathrm{i} h$ ,  $0 \le x_n \le 1$  and obtain a linear system for the coefficients

 $\boldsymbol{a} \equiv (a_0, a_1, \dots, a_{N-1})^{\top}$  as follows:

$$\sigma M_1 \boldsymbol{a} = M_2 \boldsymbol{a} + \boldsymbol{v},\tag{25}$$

where  $M_1$  and  $M_2$  are N-by-N matrices, which are calculated by evaluating the Schwarz integrals (23) and (51) at  $z_n$ , defined in (63), (64), and  $\mathbf{v} = \text{Re}[(-1+z_1, -1+z_2, \dots, -1+z_N)^\top]$ . This linear system is easily solved after  $\mathcal{Q}_n(z)$  and  $\mathcal{P}_n(z)$  defined in (61) are computed. The derivation of the linear system (25) is explained in detail in Appendix B.

Note that once  $M_1$  and  $M_2$  are calculated for geometrical parameters a and h, these matrices can be used again to calculate the temperature fields for different  $\sigma$  [34]. This decreases the computational time for evaluating the spreading resistances with fixed geometrical parameters.

The limiting case of a single-layered isotropic flux tube, i.e.,  $\sigma = 1$  is used to verify our solution provides the spreading resistance given by (1). This case corresponds to the the result is given by Veziroglu and Chandra [16] (known as the "Philip's-type" solution in the field of fluid dynamics [19]).

### 4 RESULTS

For all computations, equally-spaced collocation points between  $0 \le x \le 1$ , y = h are chosen for  $z_n$ , n = 1, ..., N. The inverse of  $\mathcal{Z}(\zeta)$  is obtained numerically by the interpolation on  $\zeta \in C_0$ . For the computation of the Schwarz integral for the unit circle (51), it is convenient to use the Fourier expansion on the unit circle. This numerical technique is explained in detail in [36].

The number of Fourier coefficients N in our approach must be carefully chosen for calculating  $\theta_1(x,h)$ . In order to determine N, we compare our numerical scheme with (1) for  $\sigma=1$  and the Fourier expansions proposed by Jain [29]. Jain expanded the solution for  $\theta_2(x,y)$  as follows:

$$\theta_2(x,y) = C_0 + D_1 y + \sum_{n=1}^{N} C_n \exp(-n\pi y) \cos(n\pi x),$$
(26)

where  $C_n$ , n = 1, ..., N are Fourier coefficients for the solution. To derive the linear system for  $C_n$ ,

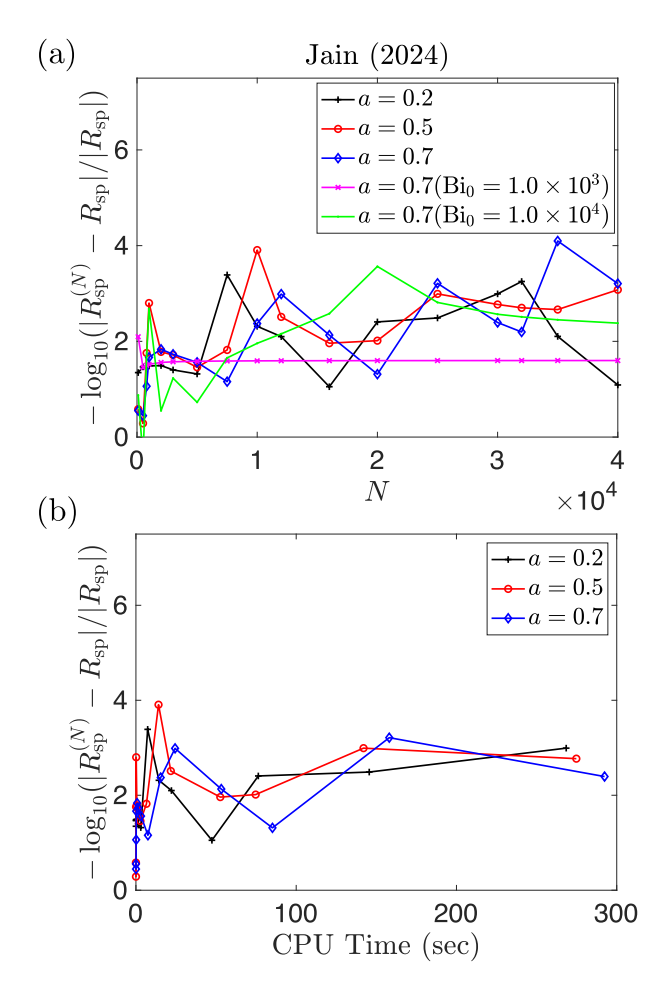


Fig. 4. (a)  $-\log_{10}$  error between Jain (2024) and Chandra and Veziroglu (1). (b) CPU time versus  $\log_{10}$  error. We used  $\mathrm{Bi_0}=1.0\times10^5$  except the magenta line and green line of the top figure. We set the height of channel h as 0.6. The data in the top figure are the same as the data in the bottom figure. The memory error occurs when we compute the coefficients of  $N=5.0\times1.0^4$ .

Jain [29] assumes a large Biot number  $Bi_0$  along the source ( $Bi_0$  at y=0) as per

$$-\frac{\partial \theta_1}{\partial y} = \operatorname{Bi}(x)\theta_1(x,0), \tag{27}$$

where

$$Bi(x) = \begin{cases} Bi_0, & 0 < x < a \\ 0, & a < x < 1. \end{cases}$$
 (28)

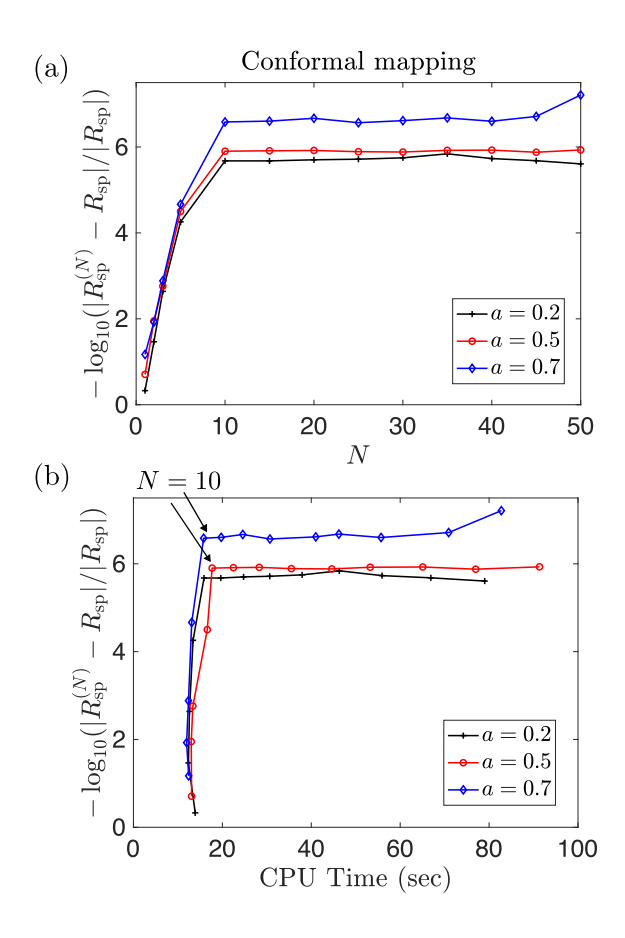


Fig. 5. (a)  $-\log_{10}$  error between our conformal mapping approach and Chandra and Veziroglu (1). Our conformal mapping approach converges to the analytical formula (1) with the error less than  $10^{-5}$ . (b) CPU time versus  $\log_{10}$  error.We set the height of channel h as 0.6. The initial computation time around 15 seconds include the computation of parameters of the triply connected domain  $D_{\zeta}$  and the calculation of  $\theta_{\rm averave}$  by using the Schwarz integral. The data in the top figure are the same as the data in the bottom figure.

A sufficiently large Biot number should be chosen so that the condition (27) becomes a good approximation of the boundary condition on the adiabatic portion, i.e.,  $-a \le x \le a$ , y = 0. We used  $\mathrm{Bi}_0 = 1.0 \times 10^5$  for our numerical experiments. We also used  $\mathrm{Bi}_0 = 1.0 \times 10^3$  and  $\mathrm{Bi}_0 = 1.0 \times 10^4$  for the numerical comparison in Figure 4.

A standard laptop (MacBook Pro 2023, Memory 18GB, Apple M3 Pro) is used for numerical computations. Computation time and accuracy depend not only on the number of Fourier coefficients N but on the number of points of the integral (20) and the Schwarz integral. We set 500 equally-spaced points between  $-1 \le \text{Re}[\zeta] \le 0$ ,  $\text{Im}[\zeta] = 0$ , in the  $\zeta$ -plane to evaluate the integral (20), and 1000 equally-spaced points to evaluate the Schwarz integral (23). We used MATLAB

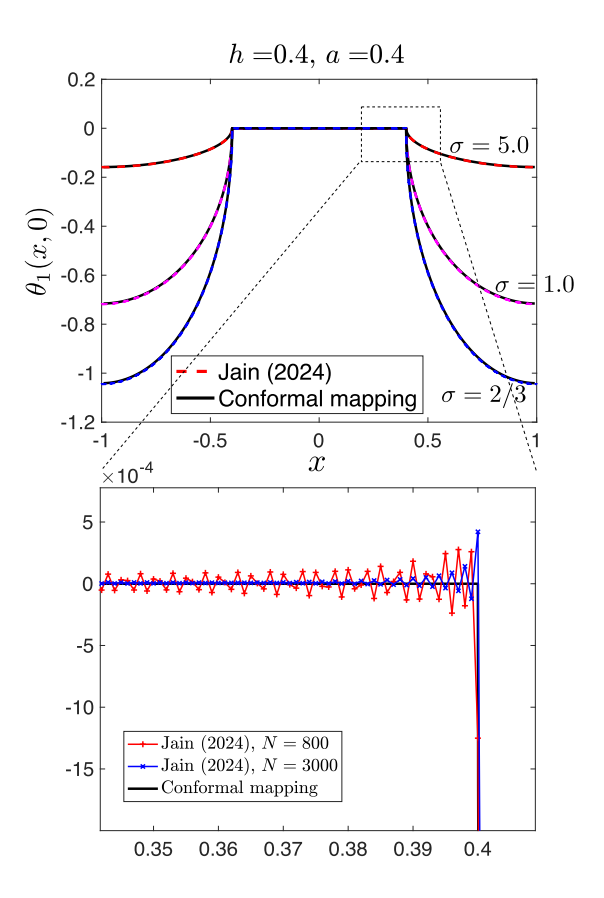


Fig. 6.  $\theta_1(x,0)$  vs. x from our approach with 30 coefficients and that of Jain [29] with 800 terms and 3000 terms for h=0.4 and a=0.4. It can be seen that the increase in the number of coefficients N deteriorates the accuracy at the singularity, i.e., x=0.4.

2024a software for all computations, i.e., the results by Jain [29] and by our Schwarz integral formulas.

Figure 4 (a) shows a  $-\log_{10}$  of the relative errors between  $R_{\rm sp}^{(N)}$  calculated by the approach by Jain up to N-1-th order of Fourier coefficients for  $\sigma=1$  and the analytical formula (1). The approach by Jain is not "convergent" since the error does not tend to zero. This is because of the finite value of  ${\rm Bi}_0$ . Moreover, when  ${\rm Bi}_0=1.0\times 10^3$ , the result is convergent but the accuracy is around  $1.0\times 10^{-2}$ . The situation for  ${\rm Bi}_0=1.0\times 10^4$  is similar but the accuracy is less than  $1.0\times 10^{-3}$ .

Figure 4 (b) shows the CPU time for calculating  $R_{\rm sp}^{(N)}$  using the approach by Jain [29] with respect to the  $-\log_{10}$  of the errors. While the results given by Jain [29] are oscillatory, his solution can be evaluated immediately (less than 1 second) when  $N\approx 1.0\times 10^3$ . However, in order to

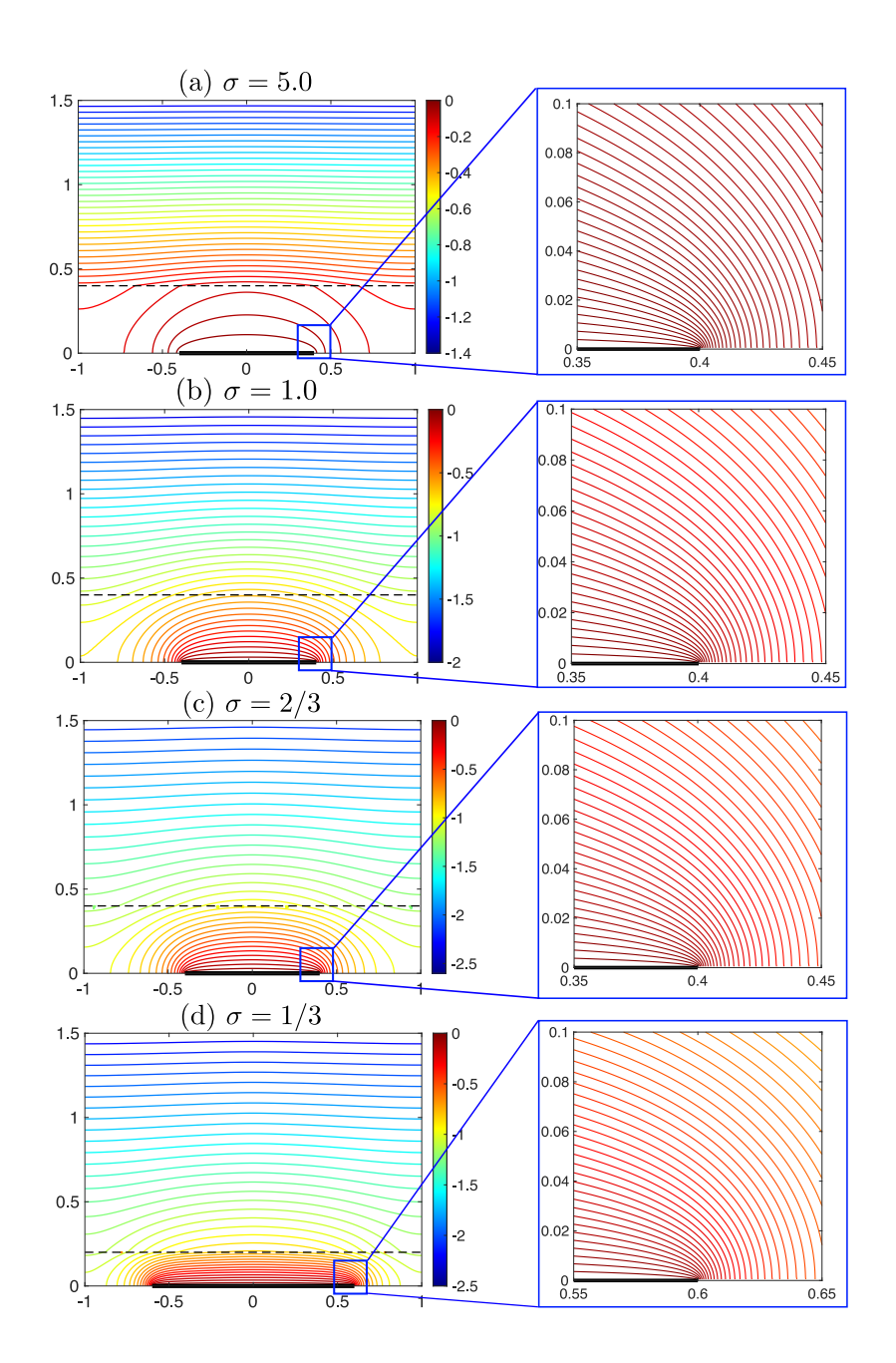


Fig. 7. Contour plots of  $\theta_1(x,y)$  and  $\theta_2(x,y)$  with different  $\sigma \equiv k_1/k_2$ . (a)  $a=0.4,\,h=0.4,\,\sigma=5.0$ , (b)  $a=0.4,\,h=0.4,\,\sigma=1.0$ , (c)  $a=0.4,\,h=0.4,\,\sigma=2/3$ , and (d)  $a=0.6,\,h=0.2,\,\sigma=1/3$ .

obtain good results by Jain (2024), many terms for the Fourier coefficients are needed.

In contrast, Figure 5 (a) shows a  $-\log_{10}$  of the errors between  $R_{\rm sp}^{(N)}$  calculated by the conformal mapping approach up to (N-1)-th order of Fourier coefficients for  $\sigma=1$  and the analytical formula (1). It can be seen that our solutions converge to the analytical formula and the errors are

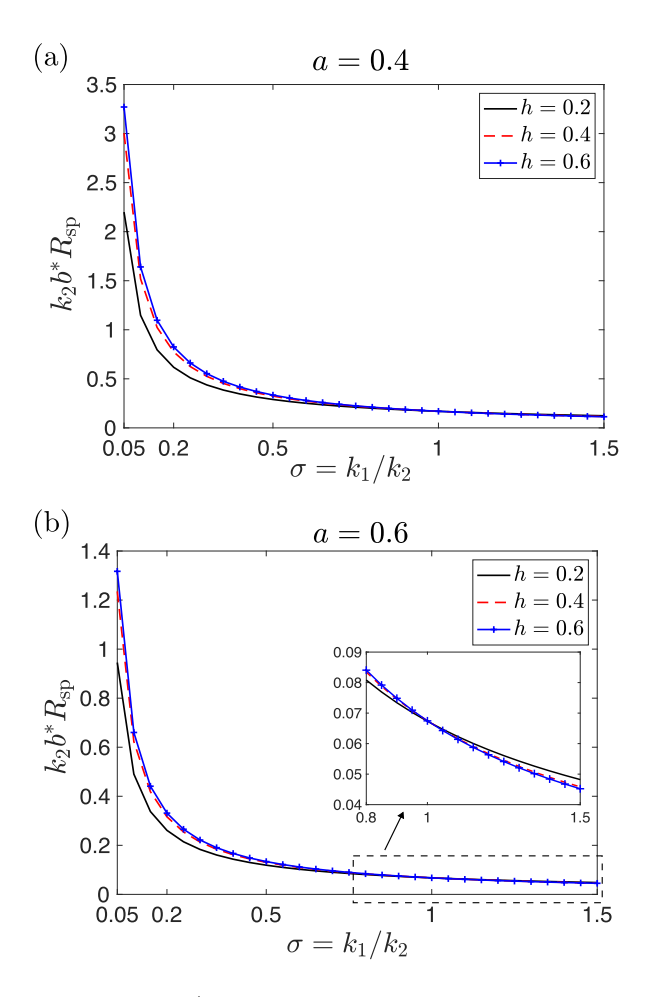


Fig. 8. Spreading resistance for different  $\sigma \equiv k_1/k_2$  with different h. The ratio of source region to period is set to be a=0.4 (a) and a=0.6 (b).

less than  $10^{-5}$  after N=10.

Figure 5 (b) shows the CPU time for calculating  $R_{\rm sp}^{(N)}$  with respect to the  $-\log_{10}$  of the errors. Our method needs to obtain appropriate parameters of  $\delta$  and q, and calculate the Schwarz integral, which takes more time than the method by Jain [29]. Based on the above, we set N=30 for all numerical experiments.

One reason for the accuracy for  $R_{\rm sp}^{(N)}$  from Jain [29] is the Gibbs phenomenon as per Figure 6, which is a comparison of  $\theta_1(x,0)$  from Jain [29] and our results. It can be seen that our results match to the results from Jain [29] for a range of values of  $\sigma$ . However, the Gibbs phenomenon is seen at the edge  $x=\pm a$  for the solutions given by Jain [29], as he used the Fourier expansions along the whole  $x\in [-1,1]$ . In general, the Gibbs phenomenon occurs when one uses Fourier

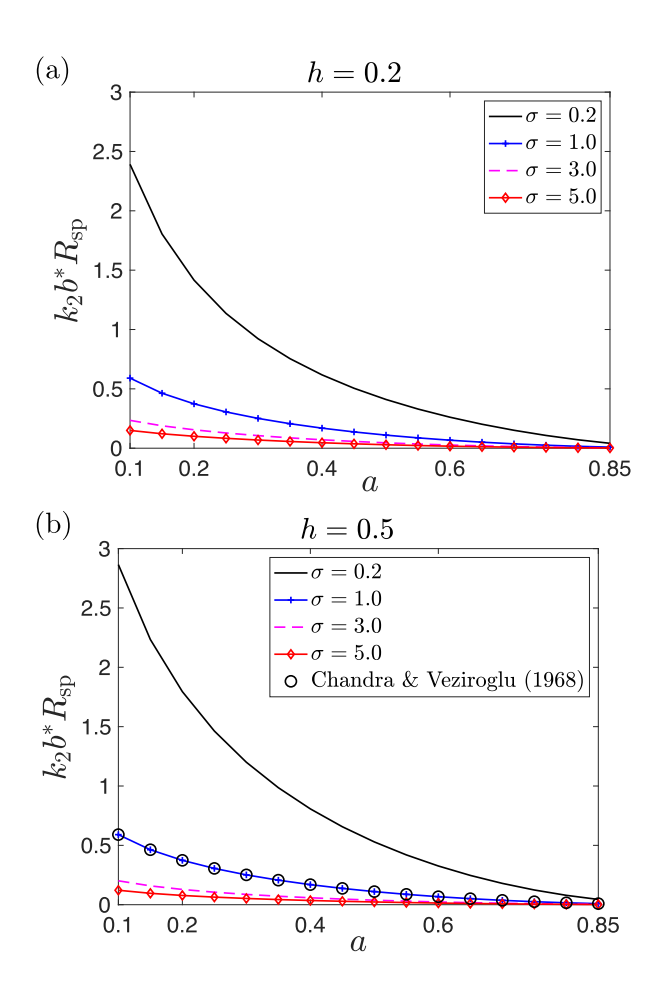


Fig. 9. Spreading resistance for different  $\sigma \equiv k_1/k_2$  with different a. The height of the first layer is set to be h=0.2 (a) and h=0.5 (b). It is also confirmed that when  $\sigma=1.0$ , the result is exactly the same as Chandra and Vezioglu (1968), plotted as black circles.

expansions for discontinuous functions such as the temperature field on y=0 in the problem at hand as explained in [38]. Hence, its representation using the Fourier expansion by Jain [29] exhibits it near the singularities at  $x=\pm a$ . This is the reason for the oscillations in the temperature field along the source plane observed in Figure 6.

Figure 7 shows contour plots of  $\theta_1(x,y)$  and  $\theta_2(x,y)$  with (a)  $\sigma=5.0$ , (b)  $\sigma=1$ , (c)  $\sigma=2/3$ , and (d)  $\sigma=1/3$ . The geometrical parameters are set to be a=0.4 and h=0.4 for cases (a), (b), and (c), and a=0.6 and h=0.2 for case (d). This figure shows our numerical calculations resolve the temperature fields around the singularities  $x=\pm a$ .

Figure 8 shows the spreading resistance for different  $\sigma \equiv k_1/k_2$  with different h. The ratio of

source region to periodicity is set to be a=0.4 (a) and a=0.6 (b). The spreading resistance decreases monotonically with respect to  $\sigma$ . All lines merge at the value (1) when  $\sigma=1.0$ , because the geometry becomes a single-layer. It can be observed that  $k_2b^*R_{\rm sp}$  increases as h increases when  $\sigma<1$ , whereas  $k_2b^*R_{\rm sp}$  decreases as h increases when  $\sigma>1$ . That is, when  $\sigma<1$  then the lower material is less conductive, and so increasing h increases the spreading resistance. However, when  $\sigma>1$ , the lower material is more conductive; therefore, increasing h decreases the spreading resistance. Figure 9 shows the spreading resistance for different  $\sigma\equiv k_1/k_2$  with different a. The height of the first layer is set to be h=0.2 (a) and h=0.5 (b). It is also confirmed that when  $\sigma=1.0$ , the result is exactly the same as Chandra and Vezioglu (1968), plotted as black circles.

We emphasize that although conventional computation tools, such as Matlab PDE Toolbox [39] and COMSOL Muliphysics 6.3.0.290 [40], may resolve the conduction problem under consideration, they require more computational resources and are less accurate than our method. Indeed, such numerical methods require a very dense mesh to compute the temperature field, especially around the square-root singularity, which they cannot fully resolve.

To validate the accuracy of our method, the coupled 2D Laplace equations are solved by using the finite element method (FEM) in COMSOL Multiphysics 6.3.0.290 [40] on a higher performance computer. The height of the second layer, i.e.,  $D_2$ , is set to be 20 instead of infinity. Tables 1, 2 and 3 compare the values  $k_2b^*R_{\rm sp}$  calculated by our approach with the results from that of Jain [29], COMSOL Multiphysics 6.3.0.290 [40], when  $\sigma=1$ ,  $\sigma=1/3$ , and  $\sigma=2$  with h=0.8 and h=0.4. The total width of the channel is set to be 2. The minimum mesh size for the discretized mesh of the finite elements is  $1.16\times 10^{-4}$  but the maximum mesh size is 0.015 for Mesh 1, 0.01 for Mesh 2, and 0.005 for Mesh 3. The relative tolerance for solving the FEM is set to be  $1.0\times 10^{-3}$  for Mesh 1 but  $1.0\times 10^{-8}$  for Mesh 2 and Mesh 3. Our conformal mapping approach shows closer agreement with Jain [29] than the COMSOL results, even for the finest mesh considered (Mesh 3) and we proceed to provide a comparison.

The values of  $k_2b^*R_{\rm sp}$  for a=0.4 and  $\sigma=1$  from the exact solution by Veziroglu & Chandra [16] (1) are displayed in the rightmost column in Table 1. It can be seen that the result by

	Conformal mapping	Jain [29]	COMSOL	Chandra & Veziroglu [16]
(Mesh 1) $h = 0.8$	0.169148	0.169727	0.162529	0.169148
(Mesh 2) $h=0.8$			0.166669	
(Mesh 3) $h = 0.8$			0.167921	
(Mesh 1) $h=0.4$	0.169155	0.169727	0.166748	0.169148

Table 1. Comparison of  $k_2b^*R_{\rm sp}$  calculated by our approach with the results by that of Jain [29], COMSOL Multiphysics [40], and Veziroglue & Chandra [16] when  $\sigma=1$  and a=1 with h=0.8 and h=0.4. The minimum mesh size for the discretized mesh is  $1.16\times 10^{-4}$  but the maximum mesh size is 0.015 for Mesh 1, 0.01 for Mesh 2, and 0.005 for Mesh 3. The relative tolerance for solving the FEM is set to be  $1.0\times 10^{-3}$  for Mesh 1 but  $1.0\times 10^{-8}$  for Mesh 2 and Mesh 3.

	Conformal mapping	Jain [29]	COMSOL
(Mesh 1) $h = 0.8$	0.504766	0.506491	0.491347
(Mesh 2) $h=0.8$			0.497376
(Mesh 3) $h = 0.8$			0.501107
(Mesh 1) $h=0.4$	0.475281	0.476860	0.461164

Table 2. Comparison of  $k_2b^*R_{\rm sp}$  between our approach, the results by that of Jain [29] and COMSOL Multiphysics. The ratio  $\sigma$  is set to be 1/3 and a=0.4. The minimum mesh size for the discretized mesh is  $1.16\times 10^{-4}$  but the maximum mesh size is 0.015 for Mesh 1, 0.01 for Mesh 2, and 0.005 for Mesh 3. The relative tolerance for solving the FEM is set to be  $1.0\times 10^{-3}$  for Mesh 1 whereas  $1.0\times 10^{-8}$  for Mesh 2 and Mesh 3.

COMSOL with Mesh 1 gives around a 4% error. Since the FEM-based approach cannot completely accommodate the singularities at  $x=\pm a$ , even with arbitrarily-small mesh size, there exist some computational errors relative to the the analytical solution (1). (Singularity subtraction could be implemented as per, e.g., Game et al. [41], but we did not do this.) It is also observed that decreasing the mesh size and restricting the relative tolerance yield more accurate results, but at the cost of increased computational resources. When  $\sigma=1/3$  and  $\sigma=2$ , a comparison between our approach and Jain [29] and COMSOL are provided in Tables 2 and 3, respectively. The differences are negligible for a sufficiently dense mesh with sufficiently low residuals.

#### 5 DISCUSSION

We have provided a new solution, based on complex analysis, to resolve a mixed (isothermal-adiabatic) boundary condition in the source plane, to obtain the spreading resistance in a com-

	Conformal mapping	Jain [29]	COMSOL [40]
(Mesh 1) $h = 0.8$	0.084873	0.085164	0.080276
(Mesh 2) $h=0.8$			0.083626
(Mesh 3) $h=0.8$			0.084256
(Mesh 1) $h=0.4$	0.088343	0.088645	0.087859

Table 3. Comparison of  $k_2b^*R_{\rm sp}$  between our approach, the results by that of [29] and COMSOL Multiphysics 6.3.0.290. The ratio  $\sigma$  is set to be 2 and a=0.4.

pound, isotropic, semi-infinite flux channel. It complements the recent and more general solution by Jain [29] that also applies for non-isotropic thermal conductivities, by fully resolving the singularities in heat flux in the source plane and achieving a more accurate spreading resistance at the expense of increased, but still negligible, computation time. Although the computation time becomes unrealistic, it would be possible to obtain the same accuracy as our results from the approach by Jain [29] with much higher  ${\rm Bi}_0$  number and a larger number of the Fourier coefficients N.

We end this article by noting that this approach is applicable for materials which have orthotropic thermal conductivity. In this case we change the coordinates  $(x,y)=(x^*/k_{1x},y^*/k_{1y})$  in  $D_1$  and  $(x,y)=(x^*/k_{2x},y^*/k_{2y})$  in  $D_2$ , where  $k_{jx}$  and  $k_{jy}$ , j=1,2 are thermal resistances with respect to  $x^*$  and  $y^*$  axis in  $D_1$  and  $D_2$ , respectively. After using the changes of coordinates above, the governing equations in the first and second layer become the 2D Laplace equation. Also, the temperature field for eccentric heat sources is available by simply modifying the conformal mapping  $\mathcal{Z}(\zeta)$  and the geometry of the predomain  $D_{\zeta}$  [36].

#### **ACKNOWLEDGEMENTS**

The first author is supported by a Postdoctoral Research Fellowships by JSPS-24KJ0041. Professor Darren Crowdy brought to our attention the work of Moizhes [13].

### **REFERENCES**

- [1] Muzychka, Y. S., and Yovanovich, M. M., 2023. *Thermal Spreading and Contact Resistance:*Fundamentals and Applications. John Wiley & Sons.
- [2] Lee, S., 1995. "Constriction/spreading resistance model for electronics packaging". In Proc. of ASME/JSME Thermal Engineering Conf., 1995.
- [3] Sauciuc, I., Chrysler, G., Mahajan, R., and Prasher, R., 2002. "Spreading in the heat sink base: Phase change systems or solid metals". *IEEE Transactions on components and packaging technologies*, **25**(4), pp. 621–628.
- [4] Mayer, M., Hodes, M., Kirk, T., and Crowdy, D., 2019. "Effect of surface curvature on contact resistance between cylinders". *Journal of Heat Transfer*, **141**(3), p. 032002.
- [5] Hodes, M., Kirk, T., and Crowdy, D., 2018. "Spreading and contact resistance formulae capturing boundary curvature and contact distribution effects". *Journal of Heat Transfer*, 140(10), p. 104503.
- [6] Enright, R., Hodes, M., Salamon, T., and Muzychka, Y., 2014. "Isoflux nusselt number and slip length formulae for superhydrophobic microchannels". *Journal of Heat Transfer*, 136(1), p. 012402.
- [7] Bagnall, K. R., Muzychka, Y. S., and Wang, E. N., 2014. "Analytical solution for temperature rise in complex multilayer structures with discrete heat sources". *IEEE Transactions on Components, Packaging and Manufacturing Technology,* **4**(5), pp. 817–830.
- [8] Smythe, W. B., 1939. Static and dynamic electricity. McGraw-Hill.
- [9] Kouwenhoven, W., and Sackett, W., 1949. "Electrical resistance offered to non-uniform current flow". *The Welding Journal Research Supplement*.
- [10] Mikic, B. B., 1967. "Thermal contact resistance.". PhD thesis, Massachusetts Institute of Technology.
- [11] Kouwenhoven, W., and SACKETT, W., 1950. "The spreading resistance of contacts". *WELD J*, **29**(10), p. 512.
- [12] Muratov, C. B., and Shvartsman, S. Y., 2008. "Boundary homogenization for periodic arrays of absorbers". *Multiscale Modeling & Simulation*, **7**(1), pp. 44–61.

- [13] MOIZHES, B., 1955. "Elektrostaticheskie usrednennye granichnye usloviya dlya metallicheskih setok". *ZHURNAL TEKHNICHESKOI FIZIKI*, **25**(1), pp. 167–176.
- [14] Hodes, M., Kane, D., Bazant, M. Z., and Kirk, T. L., 2023. "Asymptotic nusselt numbers for internal flow in the cassie state". *Journal of Fluid Mechanics*, **977**, p. A18.
- [15] Li, Z.-C., and Lu, T.-T., 2000. "Singularities and treatments of elliptic boundary value problems". *Mathematical and Computer Modelling*, **31**(8-9), pp. 97–145.
- [16] Veziroglu, T., and Chandra, S., 1968. Thermal conductance of two dimensional constrictions interim report. Tech. rep.
- [17] Veziroglu, T. N., and Huerta, M. A., 1968. "Thermal conductance of two-dimensional eccentric constrictions". In NASA Rep. No. NGR 10-007-010-SUB3. Mechanical Engineering Department, University of Miami.
- [18] Sexl, R., and Burkhard, D., 1969. "An exact solution for thermal conduction through a twodimensional eccentric constriction". In *Thermal Design Principles of Spacecraft and Entry Bodies*, J. Bevans, ed. AIAA.
- [19] Philip, J. R., 1972. "Flows satisfying mixed no-slip and no-shear conditions". *Zeitschrift für angewandte Mathematik und Physik ZAMP*, **23**(3), pp. 353–372.
- [20] Philip, J. R., 1972. "Integral properties of flows satisfying mixed no-slip and no-shear conditions". *Zeitschrift für angewandte Mathematik und Physik ZAMP*, **23**(6), pp. 960–968.
- [21] Palaparthi, R., Papageorgiou, D. T., and Maldarelli, C., 2006. "Theory and experiments on the stagnant cap regime in the motion of spherical surfactant-laden bubbles". *Journal of Fluid Mechanics*, **559**, pp. 1–44.
- [22] Peaudecerf, F. J., Landel, J. R., Goldstein, R. E., and Luzzatto-Fegiz, P., 2017. "Traces of surfactants can severely limit the drag reduction of superhydrophobic surfaces". *Proceedings* of the National Academy of Sciences, 114(28), pp. 7254–7259.
- [23] Crowdy, D. G., 2017. "Effective slip lengths for immobilized superhydrophobic surfaces". *Journal of Fluid Mechanics*, **825**, p. R2.
- [24] Schnitzer, O., 2017. "Slip length for longitudinal shear flow over an arbitrary-protrusion-angle bubble mattress: the small-solid-fraction singularity". *Journal of Fluid Mechanics*, **820**,

- pp. 580-603.
- [25] Crowdy, D. G., 2016. "Analytical formulae for longitudinal slip lengths over unidirectional superhydrophobic surfaces with curved menisci". *Journal of Fluid Mechanics*, **791**, p. R7.
- [26] Crowdy, D., 2011. "Frictional slip lengths for unidirectional superhydrophobic grooved surfaces". *Physics of Fluids*, **23**(7).
- [27] Mayer, M., Kirk, T., Hodes, M., and Crowdy, D., 2025. "Mechanical power from thermocapillarity on superhydrophobic surfaces". *Journal of Fluid Mechanics*, –(–), pp. –.
- [28] Steigerwalt Lam, L., Hodes, M., Karamanis, G., Kirk, T., and MacLachlan, S., 2016. "Effect of meniscus curvature on apparent thermal slip". *Journal of Heat Transfer*, **138**(12), p. 122004.
- [29] Jain, A., 2024. "Thermal Spreading/Constriction From an Isothermal Source Into a Multilayer Orthotropic Semi-Infinite Flux Tube". ASME Journal of Heat and Mass Transfer, 146(6), 03, p. 061401.
- [30] Muzychka, Y., 2014. "Spreading resistance in compound orthotropic flux tubes and channels with interfacial resistance". *Journal of Thermophysics and Heat Transfer*, **28**(2), pp. 313–319.
- [31] Lambert, M., and Fletcher, L., 2002. "Thermal contact conductance of non-flat, rough, metallic coated metals". *J. Heat Transfer*, **124**(3), pp. 405–412.
- [32] Kang, T. K., Peterson, G. P., and Fletcher, L., 1990. "Effect of metallic coatings on the thermal contact conductance of turned surfaces". *ASME J. Heat Transfer*, **112**, pp. 864–871.
- [33] Miyoshi, H., and Crowdy, D. G., 2023. "Generalized schwarz integral formulas for multiply connected domains". *SIAM Journal on Applied Mathematics*, **83**(3), pp. 966–984.
- [34] Miyoshi, H., Rodriguez-Broadbent, H., and Crowdy, D. G., 2024. "Numerical validation of analytical formulas for channel flows over liquid-infused surfaces". *Journal of Engineering Mathematics*, **144**(1), p. 14.
- [35] Applied and Computational Complex Analysis. "Github website". https://github.com/ACCA-Imperial.
- [36] Crowdy, D., 2020. Solving problems in multiply connected domains. SIAM.
- [37] Miyoshi, H., Rodriguez-Broadbent, H., Curran, A., and Crowdy, D., 2022. "Longitudinal flow in superhydrophobic channels with partially invaded grooves". *Journal of Engineering Math-*

- ematics, **137**(1), pp. 1–17.
- [38] Gottlieb, D., and Shu, C.-W., 1997. "On the gibbs phenomenon and its resolution". *SIAM review*, **39**(4), pp. 644–668.
- [39] Inc., T. M., 2024. Partial differential equation toolbox: 24.1 (r2024a).
- [40] Multiphysics, C., 1998. "Introduction to comsol multiphysics®". *COMSOL Multiphysics*, *Burlington, MA, accessed Feb,* **9**, p. 2018.
- [41] Game, S., Hodes, M., Keaveny, E., and Papageorgiou, D., 2017. "Physical mechanisms relevant to flow resistance in textured microchannels". *Physical Review Fluids*, **2**(9), p. 094102.
- [42] Ablowitz, M. J., and Fokas, A. S., 2003. *Complex variables: introduction and applications*. Cambridge University Press.
- [43] Crowdy, D., Kropf, E., Green, C., and Nasser, M., 2016. "The Schottky–Klein prime function: a theoretical and computational tool for applications". *IMA Journal of Applied Mathematics*, 81(3), pp. 589–628.
- [44] Crowdy, D. G., and Marshall, J. S., 2007. "Computing the Schottky-Klein prime function on the Schottky double of planar domains". *Comput. Methods Funct. Theory,* **7**, pp. 293–308.
- [45] Miyoshi, H., and Crowdy, D. G., 2023. "Estimating conformal capacity using asymptotic matching". *IMA J. Appl. Math.*, **88**(3), pp. 472–497.

### A CONNECTION BETWEEN PHILIP'S SOLUTION [19] AND CHANDRA AND VEZIROGLU [16]

When  $\sigma=1$ , i.e., there is a single material, the dimensionless temperature field ( $\theta$ ) satisfies the (2D) Laplace's equation

$$\nabla^2 \theta(x, y) = 0, \tag{29}$$

where 0 < a < b and y > 0 subject to

$$\theta(x,0) = 0, \quad x \in [-a,a],$$
 (30)

$$\frac{\partial \theta}{\partial y}(x,0) = 0, \quad x \in [-b,-a], \ x \in [a,b], \tag{31}$$

$$\frac{\partial \theta}{\partial x}(\pm b, y) = 0, \quad 0 < y < \infty,$$
 (32)

$$\frac{\partial \theta}{\partial y} \to -1 \quad \text{as } y \to \infty.$$
 (33)

For this problem, there are two well-known formula for the solution for the mixed boundary value problem. The first solution is given by Philip [19], where he used a Schwarz-Christoffel map to solve the mixed boundary value problem. The second solution is given by Chandra and Vezioglu [16] in the field of heat transfer.

For the computation of Philip's solution [19], an appropriate logarithmic branch should be chosen. We choose

$$\cos^{-1}(z) = -i\log[z - (z^2 - 1)^{1/2}] = -i\log[z - i(1 - z^2)^{1/2}].$$
 (34)

and  $\text{Im}[\log z]$  is chosen between  $-\pi < \text{Im}[\log z] \le \pi$  for -b < x < b, y > 0. Philip's solution [19]is

On Spreading Resistance for an Isothermal Source on a Compound Flux Channel

given by

$$h_{\text{Philip}}(z) = -\frac{2b}{\pi} \cos^{-1} \left( \frac{\cos(\pi z/2b)}{\cos(\pi a/2b)} \right), \tag{35}$$

where  $\cos^{-1}(z)$  is evaluated by using the second expression of (34) and a logarithmic branch is chosen between  $-\pi < \arg[z] < \pi$ .

### A relevant mathematical identity is

$$h(z) = -\frac{2b}{\pi} \cos^{-1} \left( \frac{\cos(\pi(b-z)/2b)}{\cos(\pi(b-a)/2b)} \right)$$

$$= -\frac{ib}{\pi} \log \left[ \frac{\sqrt{d^2 + f^2 \tanh^2(i\pi(b-z)/2b)} + 1}{\sqrt{d^2 + f^2 \tanh^2(i\pi(b-z)/2b)} - 1} \right] + b$$

$$= -\frac{ib}{\pi} \log \left[ \frac{\sqrt{d^2 - f^2 \tan^2(\pi(b-z)/2b)} + 1}{\sqrt{d^2 - f^2 \tan^2(\pi(b-z)/2b)} - 1} \right] + b$$

$$= -\frac{ib}{\pi} \log \left[ \frac{1 + \sqrt{1 - f^2/\cos^2(\pi(b-z)/2b)}}{1 - \sqrt{1 - f^2/\cos^2(\pi(b-z)/2b)}} \right], \tag{36}$$

where  $\theta(x,y) = \text{Im}[h(z)]$ ,  $z = x + \mathrm{i} y$  and d and f are given by

$$d \equiv \cos(\pi a/2b), \quad f \equiv \sin(\pi a/2b) = \cos(\pi (b-a)/2b).$$

The left-hand-side corresponds to Philip's-type solution [19], whereas the right-hand-side corresponds to the solution given by Mikic [10]. This equality can be proven by taking cos of the

right-hand-side and using  $d^2 + f^2 = 1$  as follows:

$$\begin{split} &\cos(-\pi h(z)/2b) \\ &= \cos\left[\frac{\mathrm{i}}{2}\log\left[\frac{\sqrt{d^2 - f^2\tan^2(\pi(b-z)/2b)} + 1}{\sqrt{d^2 - f^2\tan^2(\pi(b-z)/2b)} - 1}\right] - \frac{\pi}{2}\right] \\ &= \cos\left[\frac{\mathrm{i}}{2}\log\left[\frac{1 + \sqrt{d^2 - f^2\tan^2(\pi(b-z)/2b)}}{1 - \sqrt{d^2 - f^2\tan^2(\pi(b-z)/2b)}}\right]\right]. \end{split}$$

Multiplying both numerator and denominator by  $1+\sqrt{d^2-f^2\tan^2(\pi(b-z)/2b)}$  and using  $d^2+f^2=1$ , we have

$$\cos(-\pi h(z)/2b) 
= \cos\left[\frac{i}{2}\log\left[\frac{(1+\sqrt{1-f^2(1+\tan^2(\pi(b-z)/2b))})^2}{f^2(1+\tan^2(\pi(b-z)/2b))}\right]\right] 
= \cos\left(i\log\left[\frac{1+\sqrt{1-f^2/\cos^2(\pi(b-z)/2b)}}{f/\cos(\pi(b-z)/2b)}\right]\right) 
= \frac{\cos(\pi(b-z)/2b)}{f} = \frac{\cos(\pi(b-z)/2b)}{\cos(\pi(b-a)/2b)},$$
(37)

where we have used from the third line to the forth line

$$\cos(\mathrm{i}x) = \frac{e^{-x} + e^x}{2}.\tag{38}$$

Using the derivative of h(z) by z,

$$\frac{\partial h}{\partial z} = \frac{\sin(\frac{\pi}{2b}(b-z))}{\sqrt{\cos^2(\frac{\pi}{2b}(b-a)) - \cos^2(\frac{\pi}{2b}(b-z))}}$$
(39)

$$= -\frac{\cos(\frac{\pi z}{2b})}{\sqrt{\sin^2(\frac{\pi a}{2b}) - \sin^2(\frac{\pi z}{2b})}}.$$
(40)

Around z = a, we can expand the ratio as follows:

$$\frac{\sin^2(\frac{\pi z}{2b})}{\sin^2(\frac{\pi a}{2b})} = 1 + \frac{\pi(z-a)\cot(\frac{\pi a}{2b})}{b} + \frac{\pi^2(z-a)^2(\cot^2(\frac{\pi a}{2b}) - 1)}{4b^2} + \mathcal{O}((z-a)^3).$$
(41)

Hence we have a square-root singularity at z=a as follows:

$$\left. \frac{\partial \theta}{\partial y} \right|_{z=a} = \text{Re}\left[ \frac{\partial h}{\partial z} \right] = -\sqrt{\frac{b \cot(\frac{\pi a}{2b})}{\pi(a-z)}} + \mathcal{O}(1),$$
 (42)

which means that the derivative of  $\theta$  with respect to y has a square-root singularity at z=a.

#### **B COMPLEX ANALYSIS FORMULATION**

Let z = x + iy be a complex plane, where the subdomains  $D_1$  and  $D_2$ , bounded by symmetry boundaries, are located. Let two conformal mappings define

$$z = \mathcal{Z}(\zeta) = \frac{1}{\pi i} \log \left( \frac{\omega(\zeta, \theta_1(\infty))}{\omega(\zeta, \theta_2(\infty))} \right), \tag{43}$$

$$z = \Theta(\eta) = \frac{2}{\pi} \sin^{-1} \left( -\frac{1}{2} \left( \eta + \frac{1}{\eta} \right) \right) + ih.$$
 (44)

Also we set the inverse of the maps as  $\zeta = \xi(z)$ , and

$$\eta = \mathcal{T}(z) \equiv \Theta^{-1}(z)$$
$$= -\sin\left(\frac{\pi}{2}(z - ih)\right) + \left[1 + \sin^2\left(\frac{\pi}{2}(z - ih)\right)\right]^{1/2}.$$

These maps are illustrated in Figure 3. The first map (43) maps the upper half circle outside an inner circle labelled  $D_{\zeta}^+$  to  $D_1$ . The unit circle  $C_0^+$  is mapped to the source region, and the inner circle  $C_1$  is mapped to the interface. The domain  $D_{\zeta}$  is defined as  $D_{\zeta} = D_{\zeta}^+ \cup D_{\zeta}^-$ , where  $D_{\zeta}^-$  is a reflection of  $D_{\zeta}^+$  with respect to the x-axis as shown in Figure 3. The function  $\omega(.,.)$  is the Schottky-Klein prime function, analytic in the triply connected domain  $D_{\zeta}$ . The second map is a map from the upper-unit disc to the strip region  $D_2$ . The outer boundary is mapped to the part  $z=x+\mathrm{i}h, -1\leq x\leq 1$ , and the real axis is mapped to the vertical axes located at  $z=\pm 1+\mathrm{i}y,$  y>h. This map was previously used by Miyoshi *et al.* [37] to resolve longitudinal flows through a bounded channel over superhydrophobic surfaces with partially invaded grooves. Because  $\theta_1$  and  $\theta_2$  are harmonic functions in the z-plane, it is convenient to define  $h_1(z)=\chi_1+\mathrm{i}\theta_1$ , and  $h_2(z)=\chi_2+\mathrm{i}\theta_2$ , where  $\chi_1$  and  $\chi_2$  are complex conjugates of  $\theta_1$  and  $\theta_2$ , respectively. We resolve the boundary value problems for  $\theta_1$  and  $\theta_2$  in the following subsection.

### (i) Solution for $D_2$

Due to the far-field condition given by (16), it is convenient to set

$$h_2(z) = -(z - ih) + \hat{h}_2(z)$$
 (45)

where  $\hat{h}_2(z) \equiv \hat{\chi}_2 + \mathrm{i}\hat{\theta}_2$  is also an analytic function. As per the Cauchy-Riemann's equations,  $\hat{\theta}_2(z)$ 

On Spreading Resistance for an Isothermal Source on a Compound Flux Channel

on x = -1 and  $y \in (h, \infty)$  is

$$\frac{\partial \hat{\theta}_2}{\partial x} = -\frac{\partial \hat{\chi}_2}{\partial y} = 0. \tag{46}$$

Therefore,  $\hat{\chi}_2$  is constant on these portions. Because  $\hat{h}_2(z)$  has no singularity on the domain  $D_2$ , even at infinity, it is convenient to set  $\operatorname{Re}[\hat{h}_2(z)] = 0$  on  $z = \pm 1 + \mathrm{i} y, y \in (h, \infty)$ .

Now we define  $\mathcal{H}_2(\eta) \equiv h_2(\Theta(\eta))$ ,  $\hat{\mathcal{H}}_2(\eta) \equiv \hat{h}_2(\Theta(\eta))$ , and assume that we know the field on the interface between  $D_1$  and  $D_2$ , i.e.,  $-1 \leq x \leq 1, \ y = h$ , denoted as  $\theta_f$ . Because of the map,

$$\operatorname{Im}[\hat{\mathcal{H}}_2(\eta)] = \theta_{\mathrm{f}}(\Theta(\eta)), \quad \eta \in C_{\eta}^+. \tag{47}$$

Due to the boundary condition,

$$\operatorname{Re}[\hat{\mathcal{H}}_2(\eta)] = \frac{1}{2} [\hat{\mathcal{H}}_2(\eta) + \overline{\hat{\mathcal{H}}_2(\eta)}] = \operatorname{const}$$
(48)

on the real axis of the  $\eta$ -plane and we can set this is equal to 0 without loss of generality. Using the Schwarz reflection principle, the function  $\mathcal{H}_2(\eta)$  is analytically extended to the lower plane in the unit circle via

$$\hat{\mathcal{H}}_2(\eta) = -\overline{\hat{\mathcal{H}}_2}(\eta). \tag{49}$$

On Spreading Resistance for an Isothermal Source on a Compound Flux Channel

Hence the Dirichlet boundary value problem for  $\hat{\mathcal{H}}_2(\eta)$  is derived as follows:

$$\operatorname{Im}[\hat{\mathcal{H}}_{2}(\eta)] = \phi_{2}(\eta) \equiv \begin{cases} \theta_{f}(\Theta(\eta)), & \eta \in C_{\eta}^{+}, \\ \theta_{f}(\Theta(\overline{\eta})), & \eta \in C_{\eta}^{-} \end{cases}$$

$$(50)$$

This can be solved by the simple Schwarz integral for the unit circle [42], i.e.,

$$\hat{\mathcal{H}}_2(\eta) = \frac{1}{2\pi} \oint_{C_\eta} \frac{\phi_2(\eta')}{\eta'} \frac{\eta' + \eta}{\eta' - \eta} d\eta' + c_2, \quad c_2 \in \mathbb{R},$$

$$(51)$$

where  $c_2$  is a real constant. The far-field behavior means that  $\text{Im}[\hat{\mathcal{H}}_2(\eta)] = 0$  as  $\eta \to 0$ . This is automatically satisfied due to the nature of the boundary condition.

### (ii) Solution for $D_1$

First we define  $\mathcal{H}_1(\zeta) \equiv h_1(\mathcal{Z}(\zeta))$ . The boundary condition on y = h and the use of the map  $\mathcal{Z}(\zeta)$  yield

$$\operatorname{Im}[\mathcal{H}_1(\zeta)] = \theta_f(\mathcal{Z}(\zeta)), \quad \zeta \in C_1.$$
(52)

Also, on the portion -a < x < a, y = 0,

$$\operatorname{Im}[\mathcal{H}_1(\zeta)] = 0, \quad \zeta \in C_0^+ \tag{53}$$

The reflection on the real axis of the *z*-plane yields the boundary value problem for  $\mathcal{H}_1(\zeta)$ . Finally,

we arrive at the boundary value conditions for the triply connected domain

$$\operatorname{Im}[\mathcal{H}_{1}(\zeta)] = \phi_{1}(\zeta) = \begin{cases} 0, & \zeta \in C_{0}, \\ \theta_{f}(\mathcal{Z}(\zeta)), & \zeta \in C_{1}, \\ \theta_{f}(\mathcal{Z}(\overline{\zeta})), & \zeta \in C_{2}, \end{cases}$$

$$(54)$$

This boundary value problem can be solved by the Schwarz integral formula (55) and the integrals of the first kind  $v_1(\zeta)$  and  $v_2(\zeta)$ , i.e.,

$$\mathcal{H}_{1}(\zeta) = \frac{1}{2\pi} \sum_{j=0}^{2} \oint_{C_{j}} \hat{\phi}_{1}(\zeta') \mathrm{d}(\log \omega(\zeta, \zeta') + \log \omega(\zeta, 1/\overline{\zeta'}))$$
$$+ \alpha(v_{1}(\zeta) + v_{2}(\zeta)) + c_{1}, \quad \alpha, c_{1} \in \mathbb{R}.$$
 (55)

The parameter  $\alpha$  is determined by the coupling equations of  $h_1(z)$  and  $h_2(z)$ , and  $c_1$  is an arbitrary real parameter. The function  $\hat{\phi}$  now satisfies

$$\hat{\phi}_{1}(\zeta) = \begin{cases} -\alpha \operatorname{Im}[v_{1}(\zeta) + v_{2}(\zeta)], & \zeta \in C_{0}, \\ \theta_{f}(\mathcal{Z}(\zeta)) - \alpha \operatorname{Im}[v_{1}(\zeta) + v_{2}(\zeta)], & \zeta \in C_{1}, \\ \theta_{f}(\mathcal{Z}(\overline{\zeta})) - \alpha \operatorname{Im}[v_{1}(\zeta) + v_{2}(\zeta)], & \zeta \in C_{2}, \end{cases}$$
(56)

where  $\alpha$  is given by single-valuedness condition for multiply connected domains [36], i.e.,

$$\oint_{\partial D_{\zeta}} \hat{\phi}_1(\zeta) dv_1 = 0.$$
(57)

### (iii) Coupling $h_1(z)$ and $h_2(z)$

By using the Cauchy-Riemann equations, the second equation of (15) and integrating from

x=-1 on y=h, we have a condition for  $\chi_1$  and  $\chi_2$  as follows:

$$\sigma(\chi_1(x,h) - \chi_1(1,h)) = \chi_2(x,h) - \chi_2(1,h) + 1 - x,\tag{58}$$

where the final term of (58) comes from the constant far-field heat flux. It is convenient to set  $\chi_1(1,h)=\chi_2(1,h)=0$  without loss of generality. The method for solving this problem is as follows:

1. Expand the temperature on the boundary of the two layers  $\theta_1(x,h)$  as the Fourier coefficients:

$$\theta_1(x,h) = \sum_{n=0}^{N-1} a_n \cos n\pi x, \quad a_n \in \mathbb{R}.$$
 (59)

2. Solve  $\mathcal{H}_2(\eta)$  by using the Schwarz integral for the unit disc:

$$h_2(z) = \mathcal{H}_2(\mathcal{T}(z)) = -(z - ih) + \sum_{n=0}^{N-1} a_n \mathcal{P}_n(\mathcal{T}(z)),$$
 (60)

where  $\mathcal{P}_n(\eta)$  is a solution for the boundary value problem with a contribution of n-th order Fourier coefficient as follows:

$$\operatorname{Im}[\mathcal{P}_{n}(\eta)] = \begin{cases} \cos(n\pi \operatorname{Re}[\Theta(\eta)]), & \eta \in C_{\eta}^{+}, \\ \cos(n\pi \operatorname{Re}[\Theta(\overline{\eta})]), & \eta \in C_{\eta}^{-} \end{cases}$$
(61)

3. Solve  $\mathcal{H}_1(\zeta)$  by using the Schwarz integral formula for the triply connected domain:

$$h_1(z) = \mathcal{H}_1(\xi(z)) = \sum_{n=0}^{N-1} a_n \mathcal{Q}_n(\xi(z))$$
 (62)

where  $Q_n(\zeta)$  satisfies the boundary conditions (22).

4. Use equation (58) evaluated at N points  $z_n$  on the common boundary to obtain the linear system for the coefficients  $a_n$ . We obtain the linear equation (25) for a, where

$$M_{1} = \operatorname{Re} \begin{bmatrix} \left( Q_{0}(z_{1}) \ Q_{1}(z_{1}) \ \dots \ Q_{N-1}(z_{1}) \\ Q_{0}(z_{2}) \ \ddots \ \ddots \ Q_{N-1}(z_{2}) \\ \vdots \ \ddots \ \ddots \ \vdots \\ Q_{0}(z_{N}) \ Q_{1}(z_{N}) \dots \ Q_{N-1}(z_{N}) \right) \end{bmatrix}, \tag{63}$$

$$M_{2} = \operatorname{Re} \left[ \begin{pmatrix} \mathcal{P}_{0}(z_{1}) & \mathcal{P}_{1}(z_{1}) & \dots & \mathcal{P}_{N-1}(z_{1}) \\ \mathcal{P}_{0}(z_{2}) & \ddots & \ddots & \mathcal{P}_{N-1}(z_{2}) \\ \vdots & \ddots & \ddots & \vdots \\ \mathcal{P}_{0}(z_{N}) & \mathcal{P}_{1}(z_{N}) & \dots & \mathcal{P}_{N-1}(z_{N}) \end{pmatrix} \right], \tag{64}$$

#### C COMPUTING THE PRIME FUNCTION

Analytical formulas were derived for the solution of the problem in terms of the prime function. To plot temperature contours and calculate spreading resistances, it is necessary to be able to evaluate the prime function  $\omega(.,.)$  and there are (at least) two ways to do this. The most numerically efficient method is to make use of freely-available MATLAB codes that compute  $\omega(.,.)$  for any user-specified circular domain [35,36]. These codes are based on a numerical algorithm described in detail in [43], which extends an earlier algorithm proposed by Crowdy and Marshall [44].

Also it is known that for triply connected domains, the prime function has a convergent product

formula as

$$\omega(\zeta,\alpha) = (\zeta - \alpha) \prod_{m \in \Theta} \frac{(m(\zeta) - \alpha)(m(\alpha) - \zeta)}{(m(\zeta) - \zeta)(m(\alpha) - \alpha)}.$$
 (65)

Here each function m lies in the set of Möbius maps which denotes all elements of the free Schottky group generated by the basic Möbius maps  $\{m_j, m_j^{-1} : j=1,2\}$ , except for the identity and excluding all inverses [36]. We use this method for computing the prime function in all numerical experiments.

Following the first way to compute the prime function, we provide code for computing the prime function  $\omega(.,.)$  and the conformal map  $z=\mathcal{Z}(\zeta)$  using a "sk-prime" package [35]. After installing the skprime functions, one can use the following code to calculate the map  $\mathcal{Z}(\zeta)$ :

```
Listing 1. Matlab code for computing the map \mathcal{Z}(\zeta)
dv = [0.5i, -0.5i]; % the center
                                                                                             1
qv = [0.2, 0.2]; % the radius
                                                                                            2
D = skpDomain(dv,qv);
                                                                                             3
thinf = dv - qv.^2./(conj(dv));
                                                                                             4
\mbox{\ensuremath{\mbox{\$}}} ----- define the prime function
                                                                                             5
w1 = skprime(thinf(1) + 1i * 1e - 10, D);
                                                                                             6
w2 = skprime(thinf(2)-1i*1e-10,D);
                                                                                             7
zzeta = @(zeta) 1/pi/1i*log(w1(zeta)./w2(zeta));
                                                                                             8
```

Only six-lines of code computes the conformal map  $z=\mathcal{Z}(\zeta)$  using the prime function in triply connected domains. We note that the radii and the centers of inner discs should be determined with respect to the geometry of the first layer, i.e.,  $\delta$  and q are chosen to satisfy

$$\begin{cases} \mathcal{Z}(1) = -a, \\ \mathcal{Z}(\delta + qi) = ih. \end{cases}$$
 (66)

On Spreading Resistance for an Isothermal Source on a Compound Flux Channel

Equations (66) are solved using any non-linear solver such as Newton's method. The approximations for  $\delta$  and q with respect to the geometry are described in [45]

# LIST OF FIGURES

1	(a) Dimensional and (b) dimensionless problems for a single-material, isotropic,
	semi-infinite flux channel
2	Isothermal source on a compound, isotropic, semi-infinite, two-dimensional flux
	channel
3	Non-dimensional geometry and two conformal mappings. The map $z=\Theta(\eta)$ maps
	the upper-half disc to the period region $D_2$ , and the map $z=\mathcal{Z}(\zeta)$ maps the upper-
	half disc outside $C_1$ to the period region $D_1$
4	(a) $-\log_{10}$ error between Jain (2024) and Chandra and Veziroglu (1). (b) CPU time
	versus $\log_{10}$ error. We used $\mathrm{Bi}_0 = 1.0 \times 10^5$ except the magenta line and green line
	of the top figure. We set the height of channel $h$ as $0.6$ . The data in the top figure
	are the same as the data in the bottom figure. The memory error occurs when we
	compute the coefficients of $N=5.0\times1.0^4.$
5	(a) $-\log_{10}$ error between our conformal mapping approach and Chandra and Veziroglu (1)
	Our conformal mapping approach converges to the analytical formula (1) with the
	error less than $10^{-5}$ . (b) CPU time versus $\log_{10}$ error.We set the height of channel
	$\it h$ as $\it 0.6$ . The initial computation time around 15 seconds include the computation
	of parameters of the triply connected domain $D_\zeta$ and the calculation of $ heta_{ m averave}$ by
	using the Schwarz integral. The data in the top figure are the same as the data in
	the bottom figure
6	$\theta_1(x,0)$ vs. $x$ from our approach with 30 coefficients and that of Jain [29] with 800
	terms and 3000 terms for $h=0.4$ and $a=0.4$ . It can be seen that the increase in the
	number of coefficients $N$ deteriorates the accuracy at the singularity, i.e., $x=0.4$ 19
7	Contour plots of $\theta_1(x,y)$ and $\theta_2(x,y)$ with different $\sigma \equiv k_1/k_2$ . (a) $a=0.4,\ h=0.4,$
	$\sigma=5.0$ , (b) $a=0.4$ , $h=0.4$ , $\sigma=1.0$ , (c) $a=0.4$ , $h=0.4$ , $\sigma=2/3$ , and (d) $a=0.6$ ,
	$h = 0.2,  \sigma = 1/3.  \ldots  20$
8	Spreading resistance for different $\sigma \equiv k_1/k_2$ with different $h$ . The ratio of source
	region to period is set to be $a=0.4$ (a) and $a=0.6$ (b)

# On Spreading Resistance for an Isothermal Source on a Compound Flux Channel

9	Spreading resistance for different $\sigma \equiv k_1/k_2$ with different $a.$ The height of the first
	layer is set to be $h=0.2$ (a) and $h=0.5$ (b). It is also confirmed that when $\sigma=1.0$ ,
	the result is exactly the same as Chandra and Vezioglu (1968), plotted as black
	circles

# LIST OF TABLES

1	Comparison of $k_2b^*R_{\rm sp}$ calculated by our approach with the results by that of Jain [29],
	COMSOL Multiphysics [40], and Veziroglue & Chandra [16] when $\sigma=1$ and $a=1$
	with $h=0.8$ and $h=0.4$ . The minimum mesh size for the discretized mesh is
	$1.16\times10^{-4}$ but the maximum mesh size is $0.015$ for Mesh 1, $0.01$ for Mesh 2, and
	$0.005$ for Mesh 3. The relative tolerance for solving the FEM is set to be $1.0\times10^{-3}$
	for Mesh 1 but $1.0 \times 10^{-8}$ for Mesh 2 and Mesh 3
2	Comparison of $k_2b^*R_{\mathrm{sp}}$ between our approach, the results by that of Jain [29] and
	COMSOL Multiphysics. The ratio $\sigma$ is set to be $1/3$ and $a=0.4.$ The minimum mesh
	size for the discretized mesh is $1.16\times10^{-4}$ but the maximum mesh size is $0.015$ for
	Mesh 1, $0.01$ for Mesh 2, and $0.005$ for Mesh 3. The relative tolerance for solving the
	FEM is set to be $1.0 \times 10^{-3}$ for Mesh 1 whereas $1.0 \times 10^{-8}$ for Mesh 2 and Mesh 3 24
3	Comparison of $k_2b^*R_{\mathrm{sp}}$ between our approach, the results by that of [29] and COM-
	SOL Multiphysics 6.3.0.290. The ratio $\sigma$ is set to be 2 and $a=0.4.\ldots$ 25